Mapping Link SNRs of Wireless Mesh Networks onto an Indoor Testbed

Jing Lei, Roy Yates, Larry Greenstein, and Hang Liu
WINLAB, Rutgers University
671 Route 1 South, North Brunswick, NJ 08902, USA
{michelle, ryates, ljg, hliu}@winlab.rutgers.edu

***Abstract*— As a platform for synergistic theory-experiment exploration in the field of wireless networking, wireless testbeds have been used to facilitate a broad range of research. From the perspective of system-level wireless emulation, average link SNR is the dominant factor in the performance of a wireless link. Thus, this work seeks to develop a systematic link SNR mapping method that replicates real-world link SNRs on an indoor testbed. The challenge is to optimize the nodes' spatial configuration and transmission powers to overcome the inherent propagation differences, as expressed in terms of pathloss exponents and environmental shadowing, between the real world and a given testbed. To avoid the technical difficulty of "forward mapping" from the real world to the testbed, we have developed a reverse mapping method to turn a testbed configuration with given link SNRs into a corresponding real-world configuration. By inducing the dB link gain differences between the testbed and the real world distance-dependent path loss to have a Gaussian distribution, a close approximation to real-world log-normal shadow fading is achieved. We present results for a variety of indoor and outdoor real-world scenarios.**

I. Introduction

Motivated by the goal to advance technology innovation in the wireless networking field, the Open Access Research Testbed for Next-Generation Wireless Networks (ORBIT) project [**?**, **?**] has built a large-scale wireless network testbed which will facilitate a broad range of experimental research on novel protocols and application concepts. A component of the ORBIT system is a large two-dimensional indoor array of 802.11x radio nodes (400 nodes), which are uniformly spaced on a 20×20 meter grid. The selection of a subset of grid nodes yields a configuration that aims to emulate a wireless network in the real world.

A fundamental issue common to all testbed emulations is the replication of communication links of specified quality. We recognize that the indoor testbed does not capture all radio channel effects. For example, the radio channels on the testbed are unlikely to have significant multipath. For physical layer testing of a radio receiver design, the absence of multipath would be problematic; however, for a wireless network testbed, the difference is less significant. On the other hand, the importance of average received power or average SNR (scaling the average received power by the noise power) has been reflected in both theoretical analysis and practical measurements. Recent research [3–6] indicates that the average received power is a fundamental quantity for system-level emulations as well as statistical modeling of radio channels, whose large-scale spatial distribution is approximately log-normal and can be largely characterized by the path loss exponent and the standard deviation of shadow fading.

In practice, OFDM is widely employed in IEEE 802.11a/g wireless networks. In [7], the symbol-error rate (SER) of OFDM systems is analyzed in realistic scenarios impaired by both transmitter nonlinearity and frequency selective fading. It is shown that for a given level of transmitter nonlinearity, the SER is a function of the average SNR parameterized by the Q factor, which measures the power ratio of the signals received over the LOS path versus those signal received over the scattering paths. It can be observed from [7, Figs. 3 and 5] that the parallel SER curves have similar shape under four representative fading scenarios (hilly terrain, bad urban, typical urban and rural area), and the different Q values result in a translation of SER curves over the axis of average SNR. For example, in a hilly environment with Q factor 3 dB, the average link SNR γ is roughly equivalent to an average link SNR of $(\gamma - \epsilon)$ dB $(5 \leq \epsilon \leq 8)$ in an indoor scenario.

In [8, 9], the error performance of coded OFDM is evaluated over the frequency selective and time selective fading channels. Both analyses indicate that frequency-selectivity and time-selectivity lead to a fading margin in the average SNR, but the SER curves family maintain a similar shape over the SNR range of interest. To summarize, we claim that from the system-level perspective, the equivalence of the testbed and the real world can be established by the equivalence of average link SNRs. In a wide variety of settings, an average link SNR in a particular environment is comparable to the average link SNR in some other environment, offset by a fixed dB difference.

In this paper, we focus on the link SNR mapping methodology for static mesh networks. Specifically, our goal is to create a testbed network configuration whose link SNRs simulate the distance-dependent path gain as well as the shadowing that exist in the real world. Due to the difference in the path loss exponents, an exact "forward mapping" from the real world to the testbed cannot always be guaranteed. For example, consider the forward mapping from the real world to the testbed for 3 users. As shown in Fig. 1(a), we denote the 3 users in the real world by A, B and C, whose pairwise

This research is supported by the NSF Testbed Project (NRT Grant No. ANI-0335244).

distances are $\overline{r}_{AB} = 2\ m$, $\overline{r}_{AC} = 3\ m$ and $\overline{r}_{BC} = 4\ m$, respectively. Assume the path loss exponent in the real world is $\overline{\alpha} = 4$, but reduces to $\alpha = 2$ on the testbed. To achieve the same distance-based attenuation on the testbed, the length of the three segments will be extended to $r_{A_1B} = \overline{r}_{AB}^2$, $r_{A_2C} = \overline{r}_{AC}^2$ and $r_{BC} = \overline{r}_{BC}^2$, respectively, as shown in Fig. 1(b). However, $r_{A_1B} < |r_{BC} - r_{A_2C}|$, implying r_{A_1B}, r_{A_2C} and r_{BC} do not satisfy the triangle inequality and cannot form the side lengths of a triangle. Hence there doesn't exist an exact mapping on the testbed for users A, B and C. To generalize, we claim that the testbed cannot replicate the distance-based link gain matrix of real world mesh networks with arbitrary configurations.

Even if there exists a testbed configuration whose link gain matrix closely approximates that of a particular real-world network, we have to conduct a difficult combinatorial search for such a configuration. Moreover, if we try to match the arbitrary target values in the real world by the discrete quantities of limited size on the testbed, we have little control over the statistical properties of mapping differences. This motivates us to perform "reverse mapping" by which we turn a testbed configuration with specified link SNRs into a real-world configuration, and induce the distance-based link gain differences between the two scenarios to achieve a shadow-fading-like distribution (Gaussian in dB) that is consistent with real-world observations. The resulting "real world configuration" is in fact a fictional world of our own creation; however, it answers the question "What does a given testbed experiment represent in the real world?"

We demonstrate the method by reverse mapping the Orbit grid configurations to real-world scenarios. Moreover, the method is applicable to most typical indoor testbeds dedicated to system-level emulations. The rest of this paper is organized as follows: Section II introduces the fundamentals of link SNR mapping; Section III develops the mapping methodology; Section IV presents a set of results for different scenarios; and Section V concludes this paper.

II. Fundamentals of Link SNR Mapping

A. Path loss Modeling

In a wireless network, the propagation environment can vary from a simple line-of-sight (LOS) path to one that is characterized by various obstructions and scatterings. To model the path loss between two terminals, say A and B, which are separated by distance r_{AB} and deployed in an environment characterized by a path loss exponent α and a reference distance r_0 [3, 4, 10], we introduce an environment-dependent constant K_0 and define s_{AB} as a random shadow fading. The path gain is then given by

$$g_{AB} = K_0 \left(\frac{r_{AB}}{r_0} \right)^{-\alpha} s_{AB}. \tag{1}$$

The path gain, as used here, is the ratio of the locally averaged received power to the transmit power. We define the path loss to be the negative of the dB path gain, i.e.,

$$G_{AB} = -10 \log(g_{AB}). \tag{2}$$

It is worth noting that the factor $(r_{AB}/r_0)^{-\alpha}$ represents the deterministic contribution of distance-based attenuation, while s_{AB}, whose distribution is widely accepted as log-normal, captures the randomness of environments. Generally, a propagation environment can be characterized by K_0, the pathloss exponent α and the standard deviation σ of $10 \log (s_{AB})$. Typically, when both indoor and outdoor scenarios are considered, α ranges from 2 to 4, and σ ranges from 4 dB to 10 dB. Refined empirical path loss models introduced in [3, 4] treat both α and σ as random variables from location to location, to capture the distinctions among various environments.

B. Outline of the SNR Mapping Method

We assume the path gains in the real world are characterized by (1), with numerical values specified for K_0, r_0, α and σ. The link SNR at real-world node j due to a transmission from another node i is

$$\overline{\gamma}_{ij} = \frac{\overline{p}_i \overline{g}_{ij}}{\overline{\eta}_j}, \tag{3}$$

where $\overline{p}_i$ is the transmit power from node i, $\overline{\eta}_j$ is the receiver noise power at node j, and $\overline{g}_{ij}$ is the path gain from node i to node j, as given by (1). Note that when node i is transmitting to node j in the presence of a set of interfering transmitters $\mathcal{I}$, the signal to interference plus noise ratio (SINR) on link (i, j) is given by

$$\overline{\text{SINR}}_{ij}(\mathcal{I}) = \frac{\overline{p}_i \overline{g}_{ij}}{\sum_{k \in \mathcal{I}} \overline{p}_k \overline{g}_{kj} + \overline{\eta}_j} = \frac{\overline{\gamma}_{ij}}{\sum_{k \in \mathcal{I}} \overline{\gamma}_{kj} + 1}. \tag{4}$$

The implication of (4) is that matching the real-world and grid SNRs, $\overline{\gamma}_{ij} = \gamma_{ij}$ for all links (i, j), implies that we also match the real-world and grid SINRs for any set of interfering transmissions.

Thus the main objective is to establish a set of nodes on the laboratory grid for which the link SNRs are identical to those for a real-world network scenario that we wish to emulate. If there are N nodes in the real-world network we wish to study using the grid, then $\mathbf{\Gamma}$ is an $N \times N$ matrix, with elements $\Gamma_{ij} = 10 \log(\gamma_{ij})$, representing the received signal-to-noise ratio in dB at node j due to a transmission from node i. For clarity, we will use $\overline{(\cdot)}$ to denote quantities in the real world; thus, we seek a mapping such that $\overline{\Gamma}_{ij} = \Gamma_{ij}$ for all $i \neq j$.

The first step in the reverse mapping procedure is to specify a *node scenario* on the grid, defined by the number of nodes N and the set of node placements. The placement should be chosen so that the configuration has the qualitative features of the one desired in the real world, e.g., two clusters of nodes, or a random uniform distribution of nodes. Corresponding to the node scenario on the grid is an $N \times N$ gain matrix, $\mathbf{g}$, where $g_{ij} = g_{ji}$ for all links (i, j). For convenience only, we will assume in our computations that the inter-node path gains follow the free-space path loss (FSPL) formula

$$g_{ij} = \left(\frac{4\pi r_{ij}}{\lambda} \right)^{-2}, \tag{5}$$

where λ is the radio wavelength, in the same units as the distance, r_{ij}, between nodes i and j. Comparing (5) to (1),

we see that the FSPL formula corresponds to the case $K_0 = 1$, $r_0 = \lambda/(4\pi)$, $\alpha = 2$ and $\sigma = 0$ (no shadow fading).

The second step is to find a scenario (N-node placement) in the real world for which the distance-dependent part of $\overline{g}_{ij}$ is roughly the same as g_{ij}. To make this notion precise, we define

$$\hat{g}_{ij} = \overline{K}_0 \left(\frac{\overline{r}_{ij}}{\overline{r}_0} \right)^{-\overline{\alpha}} \tag{6}$$

as the distance dependent component of the real-world link gain $\overline{g}_{ij}$. By "roughly the same", we mean that

$$-10\log(\hat{g}_{ij}) = -10\log(g_{ij}) - \Delta_{ij}, \tag{7}$$

i.e., the distance-related real-world path loss on link (i, j) differs from the path loss on the grid by a dB offset Δ_{ij}. The central goal of our mapping is to *shape* the node placements so that the elements of the difference matrix, $\mathbf{\Delta}$, have the same first-order statistics as the assumed shadow fading. That is, each offset Δ_{ij} (note that $\Delta_{ij} = \Delta_{ji}$) has a Gaussian distribution with mean 0 and standard deviation σ. Then, by adding Δ_{ij} to $-10\log(\hat{g}_{ij})$, we achieve

$$-10\log(\overline{g}_{ij}) = -10\log(\hat{g}_{ij}) + \Delta_{ij} = -10\log(g_{ij}) \tag{8}$$

for all links (i, j). Thus the real-world link gains $\overline{g}_{ij}$ are both consistent with the statistical model of (1) and exactly equal to the grid link gains g_{ij}. The procedure for achieving this result is given in the next section.

The third step is to observe the spatial layout of real-world nodes resulting from the above gain mapping, to see if it conforms to the desired kind of spatial distribution. In general it will not, primarily because the inter-node spacings will be too small. The remedy is to stretch all distances by a common factor, τ, so that the real-world node placement has the desired spatial extent. Using the model of (1), it is easy to show that this will increase every real-world inter-node path loss by a common amount $10\overline{\alpha}\log(\tau)$ dB.

The fourth step is to assign transmit power values, $\overline{P}_i$ in dBm, for each real-world nodes i and to assign a receiver noise power, $\overline{\mathcal{N}} = 10\log\eta_i$ in dBm, assumed to be the same for all nodes. Expressing (3) in dB, the SNR at node j for the transmission from node i will be

$$\overline{\Gamma}_{ij} = \overline{P}_i - \overline{G}_{ij} - \overline{\mathcal{N}}, \tag{9}$$

where $\overline{G}_{ij} = -10\log(\overline{g}_{ij})$, as given in (2). Note that the transmit powers and the noise power are dictated by the real-world scenario one wishes to study. That is, these quantities are specified in the problem statement and are not a result of the gain mapping.

The fifth and final step is to choose the transmit powers P_i on the grid so that $\overline{\Gamma}_{ij} = \Gamma_{ij}$ for all (i, j). From (9), we see that this requires a mere scaling, namely,

$$P_i = \overline{P}_i - 10\overline{\alpha}\log(\tau) + \mathcal{N} - \overline{\mathcal{N}}. \tag{10}$$

If the grid capability is such that only a finite number of power levels can be used, the powers for the real-world scenario will be similarly constrained. This is a limitation imposed by the grid equipment, not the mapping method. In what follows, we focus on the first two steps of the mapping method, as the implementation of the last three steps is straightforward.

C. Link SNR Mapping Difference

To preserve the fidelity of real-world link SNRs, a direct but naive approach is to minimize the norm of $\overline{\mathbf{\Gamma}} - \mathbf{\Gamma}$. However, an insightful reader will notice that the above formulation in (3)-(7) ignores the contribution of shadow fading, while a realistic replication of real-world link SNRs should reflect the statistical properties of shadow fading. Therefore, our goal is to induce a log-normal distribution for $\{\Delta_{ij}\}$, which is consistent with the statistics of the shadow fading as observed in the real world. Another concern the readers may have is the geographical dimension of the real world that can be captured by a testbed of limited size, since the mismatch of the two scenarios will potentially produce a bias for $\{\Delta_{ij}\}$. In fact, the sample mean for the ensemble of link SNR mapping differences is

$$\tilde{\mu}_1 = \frac{2}{N(N-1)} \sum_{i=1}^{N} \sum_{j=i+1}^{N} \Delta_{ij}. \tag{11}$$

Noting the SNR differences can be adjusted by reconfiguring the placements and the transmission powers of nodes separately, we can always scale the transmission power appropriately to compensate for the potential bias of Δ_{ij}. Therefore it is unnecessary to constrain the network size and we will assume $\tilde{\mu}_1 = 0$ in the following.

III. Link SNR Mapping Methodology

Without loss of generality, we assume that the testbed link gains g_{ij} are given by free-space propagation. It is worth noting that this assumption is made for the numerical evaluation of our method, and is not a necessary condition for the proposed mapping methodology. Realistic deviations from this simplified assumption, as measured on an actual testbed, can be incorporated into the mapping algorithm.

A. Mapping Feasibility from Testbed to Real World

To begin with, we will prove the fact that for three nodes arbitrarily chosen from the testbed, there exists an exact mapping in the real world based on the equivalence of distance-based attenuation ($\sigma = 0$). To generalize, for a mesh network with $N > 3$ nodes, we can always partition it appropriately into three clusters and the cluster centroids will serve as the centers for the subsequent contraction mapping (Subsection III-B). By careful design of the reverse mapping procedure, we can insure the mapping differences achieve a log-normal distribution that is consistent with the real-world shadow fading effects. Since we are seeking the equivalence of link SNR between the two scenarios, a particular testbed configuration can simulate multiple real-world topologies sharing the common link SNR matrix.

Assume u, v and w stand for the pairwise distances of three nodes on the testbed and β is the ratio of pathloss exponents between the testbed and the real world. Lemma 1 establishes that when $0 < \beta < 1$, u^β, v^β and w^β satisfy the triangle

inequalities. On the basis of Lemma 1, Lemma 2 proves the existence of an exact mapping for any three nodes chosen from the testbed. Proofs appear in Appendix .

Lemma 1: For all $u, v, w > 0$ such that $|u - v| \leq w \leq u + v$ and $0 < \beta < 1$, $|u^\beta - v^\beta| < w^\beta < u^\beta + v^\beta$.

Lemma 2: If the ratio $\alpha/\overline{\alpha}$ of pathloss exponents between the testbed and the real world is less than 1, then any three nodes arbitrarily chosen from the testbed can be mapped exactly, by distance-based path losses, to the real world based on the equivalence of link SNRs.

Based on the mapping feasibility for three nodes, we will introduce a reverse mapping procedure for mesh networks, that can be split into two phases. Without loss of generality, we assume all testbed users transmit with power P dBm and all real-world users transmit with power $\overline{P}$ dBm.

B. Clustering and Contraction Mapping

For our first solution phase, we partition a given testbed configuration into L mutually exclusive clusters and then employ contraction mapping to obtain an initial real-world configuration. To obtain such a partition, we treat the coordinates of the N users as N objects in the real two-dimension space, $\Re^2$. Then we employ the K-means clustering algorithm [12] to partition the $N \times 2$ data matrix into L mutually exclusive clusters and locate the centroid of each cluster. Assume cluster l has N_l users, and the n-th user of cluster l is indexed by $k_{l,n}$. Let $\Omega_l = \{k_{l,n}\}_{n=1}^{N_l}$ represent the set of indices belonging to cluster l, then $\Omega_1 \cup \Omega_2 \cdots \cup \Omega_L = \{1, 2, \cdots N\}$ and $\Omega_i \cap \Omega_j = \emptyset$ for $i \neq j$. Based on a given distance measure (Euclidean distance, for example), the K-means clustering algorithm employs an iterative method for partitioning. As a result, the objects within each cluster are as close to each other as possible, but are as far from objects in other clusters as possible. Each cluster in the partition is characterized by its centroid and its member objects. The centroid of each cluster is defined as the point to which the sum of distances from all member objects is minimized. For the 2-D data based on the Euclidean distance, the cluster centroid is the geometric centroid, whose coordinates are the arithmetic average of those of the cluster members. Fig. 2 illustrates the application of the K-means clustering algorithm to a mesh network with 60 nodes, which is partitioned into three distinctive clusters based on the Euclidean distance.

Consider the case of $L = 3$ and let vectors $\mathbf{X}_{Q_1}$, $\mathbf{X}_{Q_2}$ and $\mathbf{X}_{Q_3}$ represent the testbed coordinates of the cluster centroids obtained from K-means clustering. In line with Lemma 2, we can map the cluster centroids from the testbed to their real-world locations $\{\overline{\mathbf{X}}_{Q_1}, \overline{\mathbf{X}}_{Q_2}, \overline{\mathbf{X}}_{Q_3}\}$ such that $g_{Q_1Q_2} = \overline{g}_{Q_1Q_2}$, $g_{Q_1Q_3} = \overline{g}_{Q_1Q_3}$ and $g_{Q_2Q_3} = \overline{g}_{Q_2Q_3}$. A simple way to obtain a good initial configuration is through contraction mapping with respect to the cluster centroid, which can be described as follows. Let $\mathbf{X}_{k_{l,n}}$ denotes the testbed coordinates of user $k_{l,n}$, i.e. the n-th user in cluster l. By contracting its distance to the cluster centroid and preserving its angles to the other users within the same cluster, we obtain its initial mapping in the real world and the coordinates are given by

$$\overline{\mathbf{X}}_{k_{l,n}}^0 = \overline{\mathbf{X}}_{Q_l} + \tau |\mathbf{X}_{k_{l,n}} - \mathbf{X}_{Q_l}|^\beta, \quad 1 \leq l \leq L, 1 \leq n \leq N_l \tag{12}$$

C. Constrained Optimization of Real-world Configurations

Starting from the initial configuration $\{\overline{\mathbf{X}}_{k_{l,n}}^0\}$, our goal is to fine-tune the nodes' real-world positions so that the mapping differences $\{\Delta_{ij}\}$ have the shadow fading like distribution consistent with the realistic environments. It is worth noting that $\{\Delta_{ij}\}$ is a function of $\overline{\mathbf{Y}}_j = \{\overline{\mathbf{X}}_{j_n}\}_{n=1}^N$, which fully characterize the real-world configuration of N receivers.

We learn from [11, 14] that the random variables derived from a particular distribution can be characterized by the high-order central moments. On the other hand, we know from (5)-(9) that the sample central moments for $\Delta_{i\,j}$ depend on the topography of the network users only. In particular, we note that *kurtosis* is a statistical measure for the outlier-proneness of a distribution, while *skewness* measures its asymmetry. Furthermore, a distinctive property of the Gaussian distribution is that both its skewness and its (excess) kurtosis are equal to 0, regardless of the mean and the variance [14]. Since the link SNRs are transformed by the log operation into the dB form, the desired log-normal distribution reduces to the Gaussian distribution for $\{\Delta_{ij}\}$. Therefore, we can formulate the mapping algorithm as a constrained optimization problem. To begin with, we introduce the following definitions for the l-th $(l = 2, 3, 4)$ sample central moment for $\{\Delta_{ij}\}$ assuming they have zero mean:

$$\tilde{\mu}_l\left(\overline{\mathbf{Y}}_j\right) = \frac{2}{N(N-1)} \sum_{i=1}^{N} \sum_{j=i+1}^{N} \left(\Delta_{ij}\right)^l. \tag{13}$$

Then, the excess sample kurtosis can be given by

$$\kappa(\overline{\mathbf{Y}}_j) = \frac{\tilde{\mu}_4\left(\overline{\mathbf{Y}}_j\right)}{\left[\tilde{\mu}_2(\overline{\mathbf{Y}}_j)\right]^2} - 3, \tag{14}$$

and the sample skewness is

$$\xi(\overline{\mathbf{Y}}_j) = \frac{\tilde{\mu}_3\left(\overline{\mathbf{Y}}_j\right)}{\left[\tilde{\mu}_2\left(\overline{\mathbf{Y}}_j\right)\right]^{\frac{3}{2}}}. \tag{15}$$

The objective function is set as the linear combination of the squared excess kurtosis and the squared skewness of the link gain differences, i.e.

$$J\left(\overline{\mathbf{Y}}_j\right) = \left[\kappa\left(\overline{\mathbf{Y}}_j\right)\right]^2 + \left[\xi\left(\overline{\mathbf{Y}}_j\right)\right]^2. \tag{16}$$

Obviously, $J\left(\overline{\mathbf{Y}}_j\right) \geq 0$, and the equality is achieved if the underlying distribution for $\{\Delta_{ij}\left(\overline{\mathbf{Y}}_j\right)\}$ is asymptotically Gaussian [14]. Therefore, given the standard deviation of the desired shadow fading, say σ_d, the optimal real-world configuration is

$$\overline{\mathbf{X}}^* = \arg\min_{\overline{\mathbf{Y}}_j} J\left(\overline{\mathbf{Y}}_j\right), \tag{17}$$

such that

$$\tilde{\mu}_2\left(\overline{\mathbf{Y}}_j\right) \leq \sigma_d. \tag{18}$$

Finally, we note that $J(\overline{\mathbf{Y}}_j)$ is a non-convex function of $\overline{\mathbf{Y}}_j$. Thus obtaining the global optimal solution $\overline{\mathbf{X}}^*$ is generally difficult. Even if advanced optimization techniques [13] are employed, it is probable that only a local optimal solution is reached. Moreover, as noted in [16] and the references therein, the quality of the solution to the nonlinear constrained optimization problem is sensitive to the initialization, and the optimum often lie close to the boundary governed by the constraints. Nevertheless, since the mapping can be conducted off-line, we can always randomize the initial configuration by a perturbation vector such that the qualified local optimal solutions, which pass the normality test and approximate the upper bound σ_d closely, can be identified and catalogued. We will show in Section IV that the above procedures work quite well.

D. Selection of Good Mappings by Hypothesis Test for Normality

From the discussion above, we know that for a given grid configuration, the optimization algorithm may turn out multiple local optimal solutions as the candidate real-world mappings, depending on the starting point of the optimization search. To evaluate the goodness of these candidates, we need to test the departure of the corresponding mapping differences from normality (Gaussian). Hypothesis tests for normality are based on different characteristics of the normal distribution, to name a few, the high order statistics such as skewness and kurtosis, cumulative distribution function and characteristic function. Due to the particular form of (16), we will consider the class of tests dedicated to the skewness and the kurtosis, such as those presented [14, 15].

IV. Experimental Results

A. Mesh Networks with a Collection of Clusters

This experiment studies the performance of the proposed reverse mapping method for mesh networks with a collection of clusters. Fig. 3 corresponds to an indoor scenario with three clusters, in which the standard deviation of the mapping differences is upper bounded by 5 dB and the K-means clustering algorithm partitions the nodes into $L = 3$ clusters for the initial testbed configuration. Fig. 4 corresponds to an outdoor scenario with two clusters, in which the constraint for standard deviation is upper bounded by 8 dB and $L = 2$ is used for the initial testbed configuration. The straight-lines in Figures 3(c) and 4(c) represent the benchmark CDF of the standard Gaussian distribution. To select the qualified good mappings, we invoke the Jarque-Bera normality test [13] and set the significance level to 5%. As can be observed from these figures, the sample kurtosis κ and the sample skewness ξ are negligibly small, and the empirical CDF approximates the straight line closely over the interval $[0.05, 0.95]$. This implies the distribution of the mapping differences is a good approximation to the desired Gaussian distribution (log-normal shadowing).

B. Mesh Networks with Uniformly Distributed Nodes

This experiment investigates the performance of the reverse mapping for a mesh network with 50 uniformly distributed nodes. Fig. 5 shows an indoor case where the standard deviation of the mapping difference is upper bounded by 5 dB. Fig. 6 shows an outdoor case where the standard deviation of the mapping difference is upper bounded by 8 dB. Similar to the prior experiments, the straight-lines of 6(c) and 7(c) represent the CDF benchmark of the standard Gaussian distribution. Similarly, the constrained optimization algorithm can induce the distribution of link SNR mapping differences to resemble that of the real-world shadow fading.

V. Conclusion

For the static mesh networks, we have proposed a novel mapping method for the link SNR, which can be formulated as a two-phase constrained optimization problem. For as many as 50 nodes, we have observed that the proposed methodology works very well for typical network topologies such as a collection of clusters or a mesh. For both indoor and outdoor scenarios, we can induce a Gaussian distribution for the differences of distance-based attenuation, which renders a good approximation to the shadow fading effects in the real world.

Appendix

Proof: Lemma 1 Let $f(x) = (1+x)^\beta - x^\beta - 1$. We have $f(0) = 0$ and $f'(x) < 0$ for all $x > 0$. Since $f(x)$ is continuous, we have that for all $x > 0$, $f(x) < 0$. Substituting u/v for x into $f(x) < 0$ yields

$$(u+v)^\beta < u^\beta + v^\beta \ . \tag{19}$$

By assumption, we have $w \le u + v$, therefore

$$w^\beta \le (u+v)^\beta < u^\beta + v^\beta. \tag{20}$$

On the other hand, by assumption we also have $|u - v| < w$. Suppose $u \ge v$ without loss of generality, then $u \le v + w$. Similar to (11), we have

$$u^\beta \le v^\beta + w^\beta \, . \tag{21}$$

Combining (11) and (19) yields

$$|u^\beta - v^\beta| \le w^\beta \le u^\beta + v^\beta. \tag{22}$$

□

Proof: Lemma 2 Suppose Q_i, $i = 1, 2, 3$, denotes the index of a node arbitrarily chosen from the testbed, whose coordinates are given by vector $\mathbf{X}_{Q_i}$. Let α and $\overline{\alpha}$ denote the pathloss exponents of the testbed and the real world, respectively, and assume the transmission power are P dB and $\overline{P}$ dB, respectively. Making the substitutions $u = |\mathbf{X}_{Q_1} - \mathbf{X}_{Q_3}|$, $v = |\mathbf{X}_{Q_2} - \mathbf{X}_{Q_3}|$ and $w = |\mathbf{X}_{Q_1} - \mathbf{X}_{Q_2}|$, and noting $|u - v| \le w \le (u + v)$, we learn immediately from Lemma 1 that there exists a triangle, say $\triangle_{Q_1Q_2Q_3}$, whose side lengths are proportional to u^β, v^β and w^β. Assuming $\beta \in (0, 1)$

and $C' > 0$ are two arbitrary constants, and denoting the coordinates of the vertex Q_i in the real world by $\{\overline{\mathbf{X}}_{Q_i}\}$, then

$$|\overline{\mathbf{X}}_{Q_i} - \overline{\mathbf{X}}_{Q_j}| = \tau |\mathbf{X}_{Q_i} - \mathbf{X}_{Q_j}|^{\beta}, \tag{23}$$

where $i, j \in \{1, 2, 3\}$ and $i \neq j$. Let $\beta_{Q_iQ_j}$ and $\overline{\beta}_{Q_iQ_j}$ denote the SNRs for link $\{\mathbf{X}_{Q_i}, \mathbf{X}_{Q_j}\}$ and link $\{\overline{\mathbf{X}}_{Q_i}, \overline{\mathbf{X}}_{Q_j}\}$, respectively. Take $\beta = \alpha/\overline{\alpha}$, we then have $g_{Q_1Q_2} = \overline{g}_{Q_1Q_2}$, $g_{Q_1Q_3} = \overline{g}_{Q_1Q_3}$ and $g_{Q_2Q_3} = \overline{g}_{Q_2Q_3}$. □

REFERENCES

[1] M. Ott, I. Seskar, R. Siracusa and M. Singh, "ORBIT Testbed Software Architecture: Supporting Experiments as a Service," *Proc. of IEEE Tridentcom*, Feb. 2005, Italy.

[2] J. Lei, R. Yates, L. Greenstein and H. Liu, "Wireless Link SNR Mapping Onto an Indoor Testbed," *Proc. of IEEE Tridentcom*, Feb. 2005, Italy.

[3] S. S. Ghassemzadeh, L. J. Greenstein, A. Kavcic, T. Sveinsson and V. Tarokh, "An Empirical Indoor Path Loss Model for Ultra-Wideband Channels," *Journal of Communications and Network*, Vol. 5, pp. 303-308, Dec. 2003.

[4] V. Erceg, L. J. Greenstein, S. Y. Tjandra, S. R. Parkoff, A. Gupta, B. Kulic, A. A. Julius, R. Bianchi, "An empirically based path loss model for wireless channels in suburban environments," *IEEE J. on Select. Areas Commun.*, Vol. 17, pp. 1205 - 1211, July 1999.

[5] J. Hansen and P. E. Leuthold, "The Mean Received Power in Ad Hoc Networks and Its Dependence on Geometrical Quantities," *IEEE Trans. Antennas Propagat.*, Vol. 52. pp. 2413-2419, Sept. 2003.

[6] J. Hansen and M. Reitzner, "Efficient Indoor Radio Channel Modeling Based on Integral Geometry," *IEEE Trans. Antennas Propagat.*, Vol. 52, pp. 2456-2463, Sept. 2004.

[7] P. Banelli, "Theoretical Analysis and Performance of OFDM Signals in Nonlinear Fading Channels," *IEEE Trans. Wireless Commun.*, Vol. 2, pp. 284-293, Mar. 2003.

[8] Y. H. Kim, I. Song, H. G. Kim, T. Chang and H. M. Kim, "Performance Analysis of a Coded OFDM System in Time-varying Multipath Rayleigh Fading Channels," *IEEE Trans. Veh. Technol.*, Vol. 48, pp. 1610-1615, Sept. 1999.

[9] Z. Liu, Y. Xin and G. B. Giannakis, "Space-time-frequency coded OFDM over frequency-selective fading channels," *IEEE Trans. Signal Processing*, Vol. 50, pp. 2465-2476, Oct. 2002.

[10] T. S. Rappaport, Wireless Communications: Principles and Practice, Prentice Hall, 1995.

[11] A. H. David and H. N. Nagaraja, Order Statistics, 3rd Edition, John Wiley, July 2003.

[12] T. Kanungo, D. M. Mount, N. Netanyahu, C. Piatko, R. Silverman and A. Y. Wu, "An efficient k-means clustering algorithm: Analysis and implementation," *IEEE Trans. Pattern Analysis and Machine Intelligence*, pp. 881-892, July 2002.

[13] P. Pardalos, Nonconvex Optimization and Its Applications, Kluwer Academic Publishers, Vol. 1, 1994.

[14] R. B. D'Agostino, A. Belanger and B. D'Agostino, "A Suggestion for Using Powerful and Informative Tests of Normality," *The American Statistician*, Vol. 44, pp. 316-321, Nov. 1990.

[15] G. Judge, R. C. Hill, W. E. Griffiths, H. Lutkepol and T. C. Lee, Introduction to the Theory and Practice of Econometrics, Wiley New York, 1998.

[16] J. E. Wieselthier, G. D. Nguyen, A. E. Ephremides and C. M. Barnhart, "Application of Optimization Techniques to a Nonlinear Problem of Communication Network Design With Nonlinear Constraints," *IEEE Trans. Automat. Contr.*, Vol. 47, pp. 1033-1038, Jun. 2003.

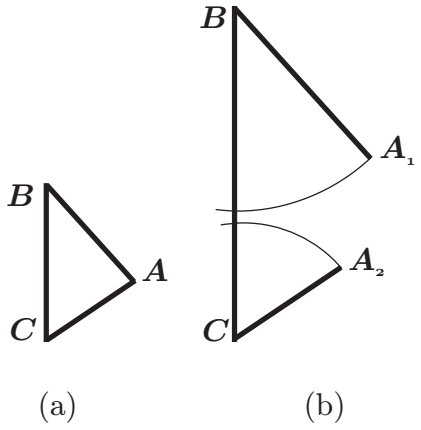

Fig. 1. Illustration of infeasibility of forward mapping from the real world to the indoor testbed for 3 users : (a) nodes A, B and C arbitrarily chosen from the real world (b) the mapping of A onto the testbed is not consistent due to the violation of triangle inequality

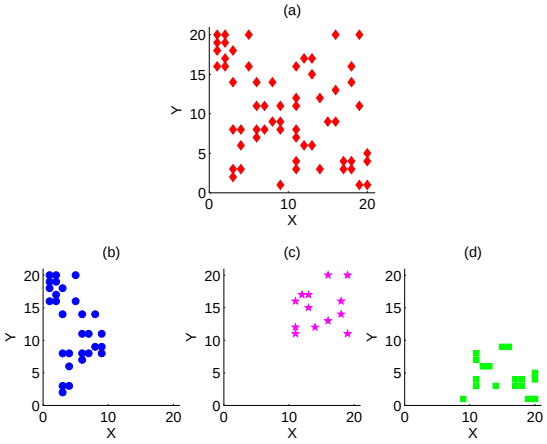

Fig. 2. Partitioning a mesh network with 60 nodes into 3 mutually exclusive clusters by K-means clustering algorithm : (a) A mesh network with 60 nodes (b) Cluster 1 (c) Cluster 2 (d) Cluster 3

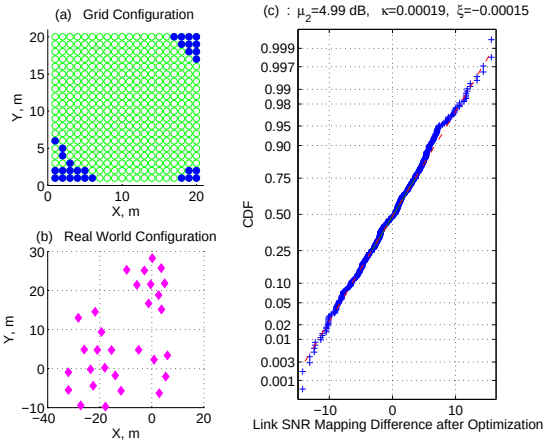

Fig. 3. Reverse mapping results of an indoor mesh network with three clusters : (a) A grid configuration with 3 clusters and a total of 30 nodes (b) A real world configuration with 3 clusters obtained by reverse mapping (c) CDF of distance-based dB path loss differences between the real world and the testbed

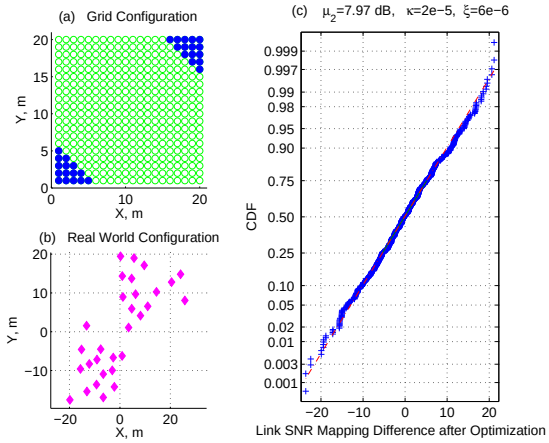

Fig. 4. Reverse mapping results of an outdoor mesh network with two clusters: (a) A grid configuration with 2 clusters and a total of 30 nodes (b) A real world configuration with 2 clusters obtained by reverse mapping (c) CDF of distance-based dB path loss differences between the real world and the testbed

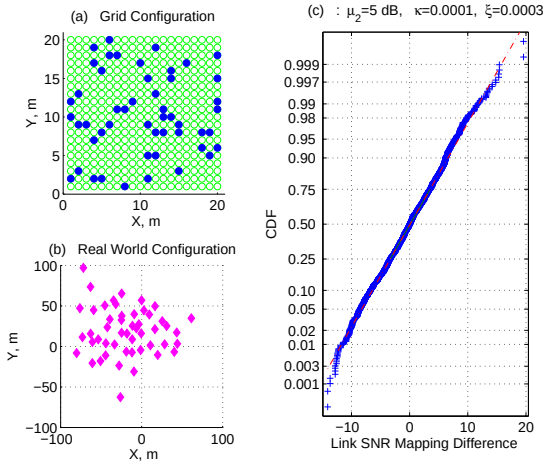

Fig. 5. Reverse mapping results for an indoor flat mesh network with 50 users: (a) A grid configuration with 50 nodes (b) A real world configuration obtained by reverse mapping (c) CDF of distance-based dB path loss differences between the real world and the testbed

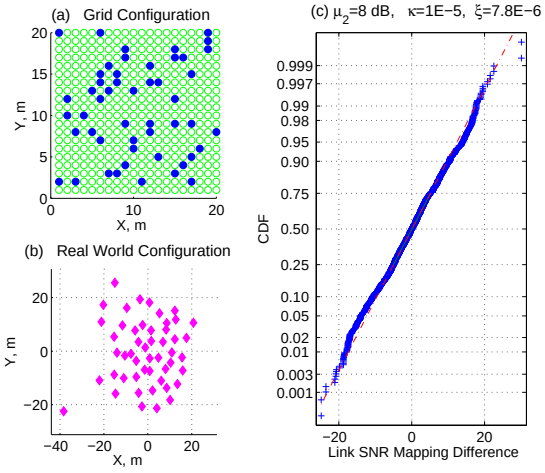

Fig. 6. Reverse mapping results for an outdoor flat mesh network with 50 users: (a) A grid configuration with 50 nodes (b) A real world configuration obtained by reverse mapping (c) CDF of distance-based dB path loss differences between the real world and the testbed